Theoretical Study on the Rank of Integral Operators for Broadband Electromagnetic Modeling From Static to Electrodynamic Frequencies

Wenwen Chai, *Student Member, IEEE*, and Dan Jiao, *Senior Member, IEEE*

***Abstract*— To facilitate the broadband modeling of integrated electronic and photonic systems from static to electrodynamic frequencies, we propose an analytical approach to study the rank of the integral operator for electromagnetic analysis, which is valid for an arbitrarily shaped object with an arbitrary electric size. With this analytical approach, we theoretically prove that for a prescribed error bound, the minimal rank of the interaction between two separated geometry blocks in an integral operator, asymptotically, is a constant for 1-D distributions of source and observation points, grows very slowly with electric size as square root of the logarithm for 2-D distributions, and scales linearly with the electric size of the block diameter for 3-D distributions. We thus prove the existence of an error-bounded low-rank representation of both surface- and volume-based integral operators for electromagnetic analysis, irrespective of electric size and object shape. Numerical experiments validated the proposed analytical approach and the resultant findings on the rank of integral operators. This paper provides a theoretical basis for employing and further developing low-rank matrix algebra for accelerating the integral-equation-based electromagnetic analysis from static to electrodynamic frequencies.**

***Index Terms*— 3-D, broadband analysis, electrodynamic analysis, integral operators, rank, theoretical analysis.**

I. Introduction

INTEGRATION is a notable trend. Integration utilizes each component's advantages and discards its disadvantages. Integration minimizes sizes, weight, power dissipation, and maximizes performance. Compared with the integration technology in the past, the integration solution in current and future integrated circuits and systems are being sought for in a much larger scale (crosscutting electronics and photonics technologies and spanning Si, GaAs, GaN, SiC, and many other semiconductor materials) and across a much wider spectrum (entire electromagnetic spectrum). It is envisioned that it is at the intersection of these technologies, materials, and spectrum that some of the greatest challenges and opportunities for integrated systems arise.

Manuscript received October 10, 2012; revised March 7, 2013; accepted April 30, 2013. Date of publication July 30, 2013; date of current version December 9, 2013. This work was supported in part by the SRC Task under Grant 1292.073, and the NSF under Award 0747578 and Award 0702567. Recommended for publication by Associate Editor M. S. Tong upon evaluation of reviewers' comments.

The authors are with the School of Electrical and Computer Engineering, Purdue University, West Lafayette, IN 47907 USA (e-mail: wwchai04@gmail.com; djiao@purdue.edu).

Color versions of one or more of the figures in this paper are available online at http://ieeexplore.ieee.org.

Digital Object Identifier 10.1109/TCPMT.2013.2261693

Driven by the design of advanced integrated systems, there exists a continued need for reducing the complexity of computational electromagnetic methods. Recently, the $\mathcal{H}$- and $\mathcal{H}^2$-matrix-based mathematical framework [1]–[3] has been introduced and further developed to accelerate both iterative and direct solutions of the integral equation-based analysis of electromagnetic problems at low as well as high frequencies, for both circuit parameter extraction and wave problems [4]–[7], [15], [19]. The resultant direct integral equation (IE) solver [5], [6] successfully solved electrically large problems of 96 wavelengths with more than 1 million unknowns in fast CPU time (<20 h in LU factorization, 85 s in one LU solution), modest memory consumption, and with the prescribed accuracy satisfied, on a single CPU running at 3 GHz.

In an $\mathcal{H}$ matrix [1]–[3], if $\mathbf{C}$ is an $m \times n$ off-diagonal block that describes the interaction between two separated subsets of the entire unknown set, it can be written as $\mathbf{C} = \mathbf{AB}^{\mathrm{T}}$ where $\mathbf{A}$ is of dimension $m \times k$, $\mathbf{B}$ is of dimension $n \times k$, and k denotes the rank of $\mathbf{C}$ with $k < m$ and $k < n$. In addition to a hierarchical low-rank representation, the $\mathcal{H}$-matrix framework also encompasses a system of fast arithmetics that permits compact storage and efficient computation of dense matrices. The $\mathcal{H}^2$ matrix is a special class of $\mathcal{H}$-matrix. It possesses a nested structure that allows for an efficient reuse of information across the entire cluster tree, and hence resulting in a better complexity than an $\mathcal{H}$-matrix-based method. To understand the actual computational complexity of an $\mathcal{H}$- or $\mathcal{H}^2$-matrix-based method for the integral equation-based analysis of high-frequency problems, and also to facilitate further acceleration of the $\mathcal{H}$- and $\mathcal{H}^2$-matrix-based computation, it becomes important to develop a theoretical understanding on the rank's dependence with electric size.

Given an accuracy requirement ε, it has been proven that the rank-r representation ($\mathbf{R}$) generated from singular value decomposition (SVD) is a minimal rank approximation of the original matrix $\mathbf{M}$ that fulfills $\|\mathbf{M} - \mathbf{R}\|_2 \leq \varepsilon$ [9]. The SVD-based minimal-rank approximation does not separate observation and source coordinates. It treats the entire matrix as a whole and finds a minimal number of vectors, and hence rank, to represent the matrix with prescribed accuracy. Our numerical experiments show that the methods, which do not generate a minimal rank approximation, such as the interpolation [4], Taylor series expansion, and plane-wave expansion-based separation of source and observation coordinates can result in a

2156-3950 © 2013 IEEE

rank that is much higher than the minimal rank required by accuracy. The rank also scales with electric size at a rate much higher than linear, as shown by existing fast multipole method (FMM)-based fast IE solvers [14] and the analysis of degrees of freedom (DF) [20] that rely on the separation of sources and observers in approximating Green's function. To be more specific, in a source-observer separated representation of the integral operator, the Green's function $g(|\vec{r}-\vec{r}'|)$, which only depends on the distance between source $\vec{r}'$ and observer $\vec{r}$, is approximated by a form of $f_1(\vec{r})f_2(\vec{r}')$, thus becoming a function of the full coordinates of $\vec{r}'$ and $\vec{r}$, yielding a full-rank representation of electrically large problems.

An SVD analysis is numerical, which makes it not feasible to find the actual rank required by accuracy for an arbitrarily large electric size. Therefore, an analytical approach, which is not restricted by computational resources and is valid for an arbitrary shape, becomes necessary to develop a theoretical understanding on the rank's dependence with electric size.

The contribution of this paper is such an analytical approach. With this approach, we theoretically prove that the minimal rank of the interaction between two separated geometry blocks in an integral-equation-based analysis of general 3-D objects, for a prescribed error bound, scales linearly with the electric size of the block diameter. For 2-D objects, the minimal rank grows very slowly with electric size as square root of the logarithm of the electric size of the problem; for 1-D objects, the minimal rank is a constant. These findings also agree with our findings on the rank of the inverse finite element matrix [12]. The proposed proof is applicable to various integral operators in electrodynamic analysis such as electric field, magnetic field, combined field, surface-, and volume-based integral operators. As the rank scales linearly with the electric size of the block diameter, while the number of unknowns in a surface- and volume-IE-based analysis scales with electric size in a quadratic, and cubic way, respectively, we prove the existence of the error-bounded low-rank representation of both surface and volume integral operators for electromagnetic analysis, irrespective of electric size and problem shape.

II. Theoretical Study

Here, we first provide a problem description, then proceed to elaborate the relationship between SVD and Fourier analysis in a linear and shift-invariant system, based on which we analytically derive the rank bound of the integral operator from the Fourier transform of Green's function. In what follows, we use a boldface letter to denote a matrix, and an italicized letter to denote a scalar.

A. Problem Description

The integral equation-based analysis of a general electromagnetic problem results in a dense linear system of equations

$$\mathbf{Z}I = V. \tag{1}$$

Consider $\mathbf{Z}^{t,s}$, an arbitrary $m \times n$ off-diagonal block of the system matrix $\mathbf{Z}$, which describes the interaction between two separated groups (t and s) of the object being analyzed, as shown in Fig. 1. The objective of this paper is to theoretically study whether there exists an error-bounded low-rank representation of $\mathbf{Z}^{t,s}$ irrespective of electric size and object shape, and if such a representation exists, how the rank scales with electric size, and hence the number of unknowns N.

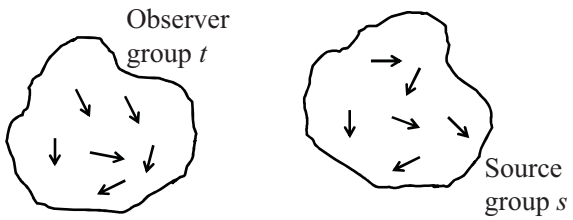

Fig. 1. Interaction between two separated groups described by an off-diagonal block in $\mathbf{Z}$.

Given an accuracy requirement ε, as shown in [9], the rank-r representation ($\mathbf{R}$) generated from SVD is a minimal rank approximation of the original matrix $\mathbf{M}$ that fulfils $\|\mathbf{M}-\mathbf{R}\|_2 \leq \varepsilon$. However, an SVD analysis is numerical. Restricted by computational resources, it cannot be used to find the actual rank required by accuracy for an arbitrarily large electric size. In this paper, we propose an analytical approach to solve this problem. In this approach, we make a connection between an SVD analysis and a Fourier analysis. By utilizing the relationship between the two analyses in a linear and shift-invariant system, we succeed in analytically revealing the rank of the integral operators and its dependence with electric size.

B. Relationship Between SVD and Fourier Analysis in a Linear Shift-Invariant System

A linear system can be modeled by the following:

$$b = \mathbf{H}f \tag{2}$$

where f and b are vectors, and $\mathbf{H}$ is a linear operator. We can perform SVD on $\mathbf{H}$ to obtain the following:

$$b = \mathbf{V}\Sigma\mathbf{U}^H f \tag{3}$$

where superscript H denotes a complex conjugate transpose, Σ is the diagonal matrix comprising singular values, and $\mathbf{V}$ and $\mathbf{U}$ are matrices comprising singular vectors. Since $\mathbf{V}$ and $\mathbf{U}$ are both unitary, we have the following:

$$\mathbf{V}^H b = \Sigma\left(\mathbf{U}^H f\right) \tag{4}$$

which can be written compactly as follows:

$$b^V = \Sigma f^U \tag{5}$$

where

$$b^V = \mathbf{V}^H b; \quad f^U = \mathbf{U}^H f. \tag{6}$$

Multiplying a unitary matrix by a vector can be thought of as projecting this vector onto the orthonormal set defined by the matrix. Thus, (5) can be viewed as representing the response b in the $\mathbf{V}$ basis (b^V), the input f in the $\mathbf{U}$ basis (f^U), and relating these two projections by a diagonal matrix (Σ).

When the operator **H** is both linear and shift invariant (LSIV), SVD turns to Fourier analysis [10]. More specifically, the singular vectors of an LSIV system are weighted Fourier basis functions (complex exponentials) and the singular values are the absolute values of the Fourier transform of the system's point spread function (impulse response function) [10], [11]. To understand this, consider an LSIV system. Because an LSIV system operator is a convolution operator [10], the response b in space domain is a convolution of the input f with an impulse response h

$$b(\vec{r}) = f(\vec{r}) * h(\vec{r}) \tag{7}$$

in which $\vec{r}$ is an arbitrary point in space. The above convolution can be converted to a simple multiplication by Fourier analysis. Thus, we have the following:

$$\mathcal{F}\big(b(\vec{r})\big) = \mathcal{F}\big(h(\vec{r})\big)\mathcal{F}\big(f(\vec{r})\big) \tag{8}$$

where $\mathcal{F}(\ )$ is a Fourier transform. We can rewrite (8) as follows:

$$b(\vec{r})^{\mathrm{FT}} = \mathcal{F}(h(\vec{r}))\, f(\vec{r})^{\mathrm{FT}} \tag{9}$$

where $b(\vec{r})^{\mathrm{FT}}$ is the representation of $b(\vec{r})$ in the Fourier basis, and $f(\vec{r})^{\mathrm{FT}}$ is the representation of $f(\vec{r})$ in the Fourier basis. In other words, we represent the input in a unitary basis (Fourier basis), we also represent the response in a unitary basis (Fourier basis), and relate the two by $\mathcal{F}(h(\vec{r}))$. From (5) and (9), the relationship between SVD and Fourier analysis can be clearly seen. The Fourier bases may be different from the SVD-generated bases. However, if the system is linear and shift-invariant, the two bases are both Fourier bases [10]. Therefore, the Fourier analysis accomplishes the SVD analysis of a linear shift-invariant system.

C. Rank Revealing Via Fourier Analysis of the Integral Operator

There exist many IE formulations for analyzing 3-D electrodynamic problems. Examples are electric field integral equation, magnetic field integral equation, combined field integral equation, each of which can be formulated in a surface- or volume-based form. The underlying integral operators are all linear and shift invariant. Therefore, we can use Fourier analysis to analytically study the rank of the integral equation-based system matrix.

The point-spread function in IE-based operators is Green's function. Without loss of generality, an integral equation-based operator can be expressed as the convolution of a certain source f with Green's function g as the following:

$$b(\vec{r}) = \int g(|\vec{r} - \vec{r}'|)\, f(\vec{r}')\, d\vec{r}' \tag{10}$$

where response b is the field at observation point $\vec{r}$, and $\vec{r}'$ is a source point. The $d\vec{r}'$ is a short notation of dl (line integral), dS (area integral), dV (volume integral) over the source domain, respectively, for 1-D, 2-D, and 3-D distribution of the source points.

Multiplying both sides of (10) by $e^{-j\vec{k}\cdot\vec{r}}$, and integrate over the observation domain $\vec{r}$, we obtain the following:

$$\int b(\vec{r}) e^{-j\vec{k}\cdot\vec{r}}\, d\vec{r} = \int \left[\int g(|\vec{r} - \vec{r}'|)\, f(\vec{r}')\, d\vec{r}' \right] e^{-j\vec{k}\cdot\vec{r}}\, d\vec{r} \tag{11}$$

which can be further written as follows:

$$\int b(\vec{r}) e^{-j\vec{k}\cdot\vec{r}}\, d\vec{r} = \int f(\vec{r}') e^{-j\vec{k}\cdot\vec{r}'}\, d\vec{r}' \times \int g(|\vec{r} - \vec{r}'|) e^{-j\vec{k}\cdot(\vec{r}-\vec{r}')}\, d(\vec{r} - \vec{r}') \tag{12}$$

and, thereby

$$B(\vec{k}) = G(\vec{k}) F(\vec{k}) \tag{13}$$

where

$$\begin{aligned} B(\vec{k}) &= \int b(\vec{r}) e^{-j\vec{k}\cdot\vec{r}}\, d\vec{r} \\ F(\vec{k}) &= \int f(\vec{r}') e^{-j\vec{k}\cdot\vec{r}'}\, d\vec{r}' \\ G(\vec{k}) &= \int g(|\vec{r} - \vec{r}'|) e^{-j\vec{k}\cdot(\vec{r}-\vec{r}')}\, d(\vec{r} - \vec{r}') \end{aligned} \tag{14}$$

in which $\vec{k} = k_x\hat{x} + k_y\hat{y} + k_z\hat{z}$. The $B(\vec{k})$, $F(\vec{k})$, and $G(\vec{k})$ are the Fourier transforms of observation fields b, sources f, and Green's function g, respectively. In (11), (12) and (14), the integration ranges for $\vec{r}$, $\vec{r}'$, and $\vec{r} - \vec{r}'$ are the ranges of the observation domain, the source domain, and the domain containing all the $\vec{r} - \vec{r}'$ points, respectively.

Equation (13), in a discrete form, can be written as follows:

$$\begin{Bmatrix} B_1 \\ B_2 \\ \vdots \\ B_p \end{Bmatrix} = \begin{pmatrix} G_1 & & & \\ & G_2 & & \\ & & \ddots & \\ & & & G_p \end{pmatrix} \begin{Bmatrix} F_1 \\ F_2 \\ \vdots \\ F_p \end{Bmatrix} \tag{15}$$

where G_i, F_i, and B_i are, respectively, $G(\vec{k})$, $F(\vec{k})$, and $B(\vec{k})$ at discrete $\vec{k}_i$ ($i = 0, 1, \ldots$), and p denotes the number of frequency points in Fourier transform.

Now consider an arbitrary source domain Ω_s that is geometrically disconnected from an arbitrary observation domain Ω_t. The number of DF in the source domain is denoted by n, while that in the observation domain is denoted by m. The matrix block corresponding to the interaction between Ω_s and Ω_t is an off-diagonal block in the system matrix **Z** resulting from an IE-based analysis of an electromagnetic problem. Denote this block by $\mathbf{Z}^{t,s}$. Thus, we have the following:

$$b_{m\times 1} = (Z^{t,s})_{m\times n} f_{n\times 1} \tag{16}$$

in which the subscripts denote the dimension of the corresponding vector or matrix. Given a prescribed accuracy, the minimal rank of $\mathbf{Z}^{t,s}$ can be numerically determined by SVD. Next, we show how to analyze the rank of $\mathbf{Z}^{t,s}$ analytically by the Fourier analysis of the integral operator.

From (14), the B vector in (15) can be written as follows:

$$\begin{Bmatrix} B_1 \\ B_2 \\ \vdots \\ B_p \end{Bmatrix} = \mathbf{B}_{p\times m} \begin{Bmatrix} b_1 \\ b_2 \\ \vdots \\ b_m \end{Bmatrix} = \mathbf{B}_{p\times m} b_{m\times 1} \tag{17}$$

where $\mathbf{B}_{p\times m}$ is the $p\times m$ matrix that projects the observations b onto the space of Fourier modes. If using a pulse basis to represent b, the ij-th matrix element of $\mathbf{B}_{p\times m}$ can be readily identified from the first row of (14) as follows:

$$\mathbf{B}_{i,j}=\int_j e^{-j\vec{k}_i\cdot\vec{r}}\,d\vec{r},\quad 1\le i\le p,\quad 1\le j\le m \tag{18}$$

where the integral is evaluated on the domain occupied by the jth observer. For 1-D, 2-D, and 3-D distribution of the observers, such a domain is a segment, a surface, and a volume, respectively.

Similarly, from (14), the F vector in (15) can be written as follows:

$$\begin{Bmatrix} F_1\\ F_2\\ \vdots\\ F_p\end{Bmatrix}=\mathbf{F}_{p\times n}\begin{Bmatrix} f_1\\ f_2\\ \vdots\\ f_n\end{Bmatrix}=\mathbf{F}_{p\times n}f_{n\times 1} \tag{19}$$

where $\mathbf{F}_{p\times n}$ is the $p\times n$ matrix that projects the sources f onto the space of Fourier modes. Its ij-th matrix element can also be readily identified from (14) as follows:

$$\mathbf{F}_{i,j}=\int_j e^{-j\vec{k}_i\cdot\vec{r}'}\,d\vec{r}',\quad 1\le i\le p,\quad 1\le j\le n \tag{20}$$

where the integral is evaluated on the domain occupied by the jth source.

Substituting (17) and (19) into (15), we obtain the following:

$$\mathbf{B}b=\mathbf{G}(\mathbf{F}f) \tag{21}$$

where $\mathbf{G}$ in boldface denotes the diagonal matrix composed of the Fourier coefficients of Green's function shown in (15). If $\mathbf{B}$ is unitary, then

$$b=(\mathbf{B}^{\mathrm{H}}\mathbf{G}\mathbf{F})f. \tag{22}$$

In the context of matrix computation, the source and observation domain represented by an off-diagonal block are both finite. In addition, they may not span a period used for evaluating the discrete Fourier transform. Although Fourier bases are unitary, if a subset of these bases is chosen at selected source and observation points, neither $\mathbf{B}$ nor $\mathbf{F}$ is unitary. In this case, (21) can be written as follows:

$$b=(\mathbf{B}^{\mathrm{H}}\mathbf{B})^{-1}(\mathbf{B}^{\mathrm{H}}\mathbf{G}\mathbf{F})f. \tag{23}$$

With p chosen to be larger than m, $(\mathbf{B}^{\mathrm{H}}\mathbf{B})$ is invertible. If $(\mathbf{B}^{\mathrm{H}}\mathbf{B})$ is not invertible, we can also write $\mathbf{B}$ as follows:

$$\mathbf{B}=\mathbf{U}_B\Sigma_B\mathbf{V}_B^H \tag{24}$$

which is the SVD of $\mathbf{B}$. Then, we have the following:

$$b=(\mathbf{V}_B\Sigma_B^{-1}\mathbf{U}_B^H\mathbf{G}\mathbf{F})f. \tag{25}$$

Therefore, we obtain the following:

$$\mathbf{Z}^{t,s}=(\mathbf{V}_B\Sigma_B^{-1}\mathbf{U}_B^H\mathbf{G}\mathbf{F}). \tag{26}$$

Thus, it is clear that if $\mathbf{B}$ and $\mathbf{F}$ are unitary, then the singular values of $\mathbf{Z}^{t,s}$ are nothing but the absolute values of $\mathbf{G}$'s entries, which are the Fourier coefficients of Green's function. In general cases where $\mathbf{B}$ and $\mathbf{F}$ may not be unitary, although the singular values are not the Fourier coefficients any more, the rank of $\mathbf{Z}^{t,s}$ is still bounded by the rank of diagonal matrix $\mathbf{G}$ since the rank of a matrix product is no greater than any of the matrices being multiplied. Therefore, we can analyze the Fourier transform of Green's function to analytically study the rank of $\mathbf{Z}^{t,s}$.

D. Rank Determined from an Analytical Fourier Analysis of the Green's Function

The Green's function for a general 3-D problem can be written as follows:

$$g(|\vec{r}-\vec{r}'|)=\frac{e^{-jk_0|\vec{r}-\vec{r}'|}}{4\pi|\vec{r}-\vec{r}'|} \tag{27}$$

where $\vec{r}'$ is a source point, $\vec{r}$ is an observation point, and k_0 is the wave number corresponding to a frequency being studied. Let

$$\vec{R}=\vec{r}-\vec{r}'=R\hat{R} \tag{28}$$

with R being the magnitude of the distance vector $\vec{R}$ and $\hat{R}$ a unit vector along $\vec{r}-\vec{r}'$ direction, (27) can be further written as follows:

$$g(R)=\frac{e^{-jk_0R}}{4\pi R}. \tag{29}$$

The above Green's function satisfies the following partial differential equation in an infinite space:

$$\nabla^2 g+k_0^2 g=\delta(\vec{r}-\vec{r}'). \tag{30}$$

Its Fourier transform can be analytically obtained as follows.

First, we represent the right hand side (RHS) of (30) by its Fourier transform

$$\delta(\vec{r}-\vec{r}')=\frac{1}{(2\pi)^3}\iiint e^{jk_x(x-x')}e^{jk_y(y-y')}\times e^{jk_z(z-z')}\,dk_x\,dk_y\,dk_z. \tag{31}$$

Similarly, we write Green's function g as follows:

$$g(\vec{r}-\vec{r}')=\frac{1}{(2\pi)^3}\iiint G(k)e^{jk_x(x-x')}e^{jk_y(y-y')}\times e^{jk_z(z-z')}\,dk_x\,dk_y\,dk_z \tag{32}$$

where $G(k)$ is the Fourier transform of g. Substituting (32) into the left hand side of (30), we obtain the following:

$$\begin{aligned}\nabla^2 g+k_0^2 g&=\frac{1}{(2\pi)^3}\iiint G(k)\nabla^2\\&\quad\times\left[e^{jk_x(x-x')}e^{jk_y(y-y')}e^{jk_z(z-z')}\right]dk_x\,dk_y\,dk_z\\&\quad+\frac{1}{(2\pi)^3}\iiint k_0^2G(k)e^{jk_x(x-x')}e^{jk_y(y-y')}\\&\quad\times e^{jk_z(z-z')}\,dk_x\,dk_y\,dk_z\\&=\frac{1}{(2\pi)^3}\iiint(-k^2+k_0^2)G(k)e^{jk_x(x-x')}\\&\quad\times e^{jk_y(y-y')}e^{jk_z(z-z')}\,dk_x\,dk_y\,dk_z\end{aligned} \tag{33}$$

where

$$k^2=k_x^2+k_y^2+k_z^2. \tag{34}$$

Since (33) is equal to (31), we obtain the Fourier transform of Green's function as the following:

$$G(k) = \frac{1}{k_0^2 - k^2}. \tag{35}$$

The above approach was actually one of the methods used to derive Green's function in history, also known as Ohm-Rayleigh method [13, p. 30], which is also given in [18, p. 55]. In addition, (35) provides another proof of the interior resonance problem associated with IE formulations [16], since it shows that if k_0 is the same as one of the ks, the integral operator becomes singular.

If both source points $\vec{r}'$ and observation points $\vec{r}$ are distributed in a 2-D domain, without loss of generality, assume $z = z'$. From (33), since the term operated on by ∇^2 is $e^{jk_x(x-x')}e^{jk_y(y-y')} \cdot 1$, we obtain the following:

$$k^2 = k_x^2 + k_y^2. \tag{36}$$

Note that the above does not suggest that $\partial/\partial z = 0$ because when the RHS of (32) is integrated out, we obtain $\delta(z - z')$. If both source points $\vec{r}'$ and observation points $\vec{r}$ are distributed in a 1-D domain satisfying $z = z'$ and $y = y'$, from (33), we have the following:

$$k^2 = k_x^2. \tag{37}$$

Again, the above does not suggest that $\partial/\partial y = \partial/\partial z = 0$ because when (32) is integrated out, we obtain $\delta(y - y')\delta(z - z')$. As can be seen from the above derivation, the Fourier transform of Green's function for 1-D, 2-D, and 3-D distributions of source points and observation points has the same form as that shown in (35). The only difference is in k^2.

Now, we are ready to determine the rank of $\mathbf{G}$ in (26). The $\mathbf{G}$ is the diagonal matrix shown in (15), the entries of which are given in (14), which are the Fourier coefficients of Green's function

$$G(\vec{k}_i) = \int g(|\vec{r} - \vec{r}'|)e^{-j\vec{k}_i \cdot (\vec{r} - \vec{r}')}\, d(\vec{r} - \vec{r}'). \tag{38}$$

For a finite source-observation domain, the geometrical identity defined by $(\vec{r} - \vec{r}')$ is finite. Take a 3-D $(\vec{r} - \vec{r}')$ domain as an example, (38) can be explicitly written as follows:

$$G(\vec{k}_i) = \int_{\varphi_1}^{\varphi_2} \int_{\theta_1}^{\theta_2} \int_{R_1}^{R_2} \frac{e^{-jk_0R}}{4\pi R} e^{-j\vec{k}_i \cdot \vec{R}} R^2 \sin\theta \, dr \, d\theta \, d\varphi \tag{39}$$

where the upper and lower limits describe the region that $(\vec{r} - \vec{r}')$ occupies. If $(\vec{r} - \vec{r}')$ has multiple disconnected regions, then the matrix block corresponding to such a source-observation interaction is the union of the matrix block in each separated region. Then for each separated region, we can analyze the rank of the corresponding matrix block via (39). The rank of a matrix sum is bounded by the sum of the rank of each matrix [9]. Therefore, the sum of the rank of the matrix block for each separated region is the upper bound of the rank of the entire matrix block associated with the interaction between $\vec{r}'$ and $\vec{r}$.

Let $(\varphi_1, \varphi_2) = (0, 2\pi)$, $(\theta_1, \theta_2) = (0, \pi)$, and $R_1 \to 0$, $R_2 \to \infty$. Then (39) becomes (35), and hence

$$G(\vec{k}_i) = \frac{1}{k_0^2 - (k_{xi}^2 + k_{yi}^2 + k_{zi}^2)} \tag{40}$$

where

$$\begin{aligned} k_{xi} &= m\frac{2\pi}{D} = \frac{m\pi}{a} \\ k_{yi} &= n\frac{2\pi}{D} = \frac{n\pi}{a} \\ k_{yi} &= p\frac{2\pi}{D} = \frac{p\pi}{a} \end{aligned} \tag{41}$$

in which m, n, and p are integer numbers, D is the maximal size of the problem along x-, y-, and z-direction, and a is half of D. In what follows, we use (40) and its corresponding 2-D and 1-D forms to analytically analyze the rank of $\mathbf{G}$ because the rank of a smaller $(\vec{r} - \vec{r}')$ domain determined by (39) is bounded by the rank dictated by (40).

Without performing a detailed quantitative analysis, from (40), we already can predict the existence of a low-rank representation of Green's function. The reason is straightforward. Given a k_0^2, not all of the Fourier modes have a large Fourier coefficient, only those whose wave number square (k_i^2) are the closest to k_0^2 have the largest Fourier coefficients, whereas others can be truncated based on the magnitude of their Fourier coefficients and a prescribed accuracy. The total number of Fourier modes representing a function defined on a surface and that defined in a volume is, respectively, proportional to (electric size)^2 and (electric size)^3. Thus, the total number of Fourier modes is linearly proportional to N. However, Green's function is different from an arbitrary function that depends on x, y, and z, because of its R-only dependence, its Fourier transform has a special form shown in (40). Therefore, only a subset of Fourier modes needs to be used to represent the Green's function for a given accuracy, while the rest can be discarded without sacrificing the prescribed accuracy. Hence the rank of $\mathbf{G}$ is less than N, thus being low rank. In addition, (40) also reveals why the rank of a 2-D problem is, in general, less than that of a 3-D distribution of sources and observers. This is because in the former, the Fourier modes are distributed on a 2-D grid as can be seen from (36) and (41), whereas in the latter; the Fourier modes are distributed on a 3-D lattice. Thus, the number of Fourier modes satisfying a prescribed accuracy in a 2-D case is smaller than that in a 3-D case. The above analysis is conceptual. Next, we provide a quantitative analysis of the rank of $\mathbf{G}$ and its dependence with electric size.

Given an accuracy requirement ε, the rank of diagonal matrix $\mathbf{G}$ is the number of Fourier coefficients $G_i = G(k_i)$ satisfying the following criterion:

$$\frac{G_i}{\max\{G_i\}} = \frac{1/|k_i^2 - k_0^2|}{\max\{1/|k_i^2 - k_0^2|\}_i} \geq \varepsilon. \tag{42}$$

Since the maximum of $1/|k_i^2 - k_0^2|$ occurs at the minimum of $|k_i^2 - k_0^2|$, (42) can be written as follows:

$$\frac{1/|k_i^2 - k_0^2|}{1/|k_i^2 - k_0^2|_{\min}} \geq \varepsilon. \tag{43}$$

Let

$$\Delta_{\min} = |k_i^2 - k_0^2|_{\min}. \tag{44}$$

We have

$$|k_i^2 - k_0^2| \le \Delta_{\min}/\varepsilon \tag{45}$$

with

$$k_i^2 = \left[(m\pi)^2 + (n\pi)^2 + (p\pi)^2\right]/a^2 \tag{46}$$

$$k_i^2 = \left[(m\pi)^2 + (n\pi)^2\right]/a^2 \tag{47}$$

$$k_i^2 = \left[(m\pi)^2\right]/a^2 \tag{48}$$

for 3-D, 2-D, and 1-D distribution of sources and observers, respectively.

To determine the rank from (45), we can find out the maximum displacement $\Delta_k > 0$ satisfying

$$(k_0 + \Delta_k)^2 - k_0^2 \le \Delta_{\min}/\varepsilon \tag{49}$$

and then compute the number of modes that can exist between k_0 and $k_0 + \Delta_k$. For the modes satisfying (45) and having k_i^2 smaller than k_0^2, a similar analysis can be performed.

In 1-D cases, as $k_i = (m\pi)/a$, the distance between two adjacent wave number k_i is a constant. The number of Fourier modes between k_0 and $k_0 + \Delta_k$ is thus proportional to Δ_k. Therefore, the rank in 1-D cases can be written as follows:

$$\text{Rank}|_{1\text{D}} \sim \Delta_k. \tag{50}$$

In 2-D cases, as the number of Fourier modes having a wave number between k_0 and $k_0 + \Delta_k$ is proportional to the area of a ring with inner radius of k_0 and outer radius of $k_0 + \Delta_k$. Thus, the rank in 2-D cases can be written as follows:

$$\text{Rank}|_{2\text{D}} \sim (k_0 + \Delta_k)^2 - k_0^2 = 2k_0\Delta_k + \Delta_k^2. \tag{51}$$

In 3-D cases, the number of Fourier modes having a wave number between k_0 and $k_0 + \Delta_k$ is proportional to the volume of a spherical ring with inner radius of k_0 and outer radius of $k_0 + \Delta_k$. Thus

$$\text{Rank}|_{3\text{D}} \sim (k_0 + \Delta_k)^3 - k_0^3 = 3k_0^2\Delta_k + 3k_0\Delta_k^2 + \Delta_k^3. \tag{52}$$

From the above, it can be seen that the rank's dependence with electric size is determined by Δ_k's dependence with electric size. This question was thoroughly studied in [12]. In fact, the Fourier transform of Green's function has a direct relationship with the inverse of the finite element matrix by comparing (35) with the inverse of the finite element matrix shown in [12]. It is proved in [12] that Δ_k for 1-D, 2-D, and 3-D modes satisfying (49), for a given ε, asymptotically scales with frequency in the following way:

$$\Delta_k|_{1\text{D}} \sim O(1) \tag{53}$$

$$\Delta_k|_{2\text{D}} \sim O(\sqrt{\log k_0}/k_0) \tag{54}$$

$$\Delta_k|_{3\text{D}} \sim O(1/k_0). \tag{55}$$

Substituting them into (50)–(52), we obtain the following:

$$\text{Rank}|_{1\text{D}} = \text{constant} \tag{56}$$

$$\text{Rank}|_{2\text{D}} \sim O(\sqrt{\log k_0}). \tag{57}$$

$$\text{Rank}|_{3\text{D}} \sim O(k_0). \tag{58}$$

Thus, for 1-D problems, for a prescribed error bound, the rank is a constant; for 2-D problems, the asymptotic scaling rate of the rank is less than linear; while for 3-D problems, the rank increases linearly with the electric size of the problem. The theoretical results shown in (56)–(58) are also numerically verified by finding out the number of modes having wave numbers shown in (46)–(48) and meanwhile satisfying (45) [12].

The above asymptotic growth rate of the rank is for electrically large problems, the electric size of which approaches infinity. For static, i.e., frequency independent problems, the k_0 is zero in (35). Thus, $G(k)$ becomes frequency independent. Its largest magnitude occurs at $k = 0$, which can be evaluated from $G(0) = \int g(|\vec{r}-\vec{r}'|)\, d(\vec{r}-\vec{r}')$ instead of using (35) as (35) requires a nonzero k. Therefore, given an accuracy requirement ε, by setting $|G_i|/|G(0)| < \varepsilon$, it can be readily found that the rank of static problems is a constant irrespective of problem size. This agrees with the rank of existing fast algorithms when applied to the analysis of static and electrically small problems.

It is worth mentioning that although the source-observer separated representation of Green's function used in an FMM-based method results in a rank's growth rate much higher than that shown in (56)–(58), the number of spherical harmonics required to approximate the original Green's function for a given accuracy, for the interaction between two separated blocks, is also shown to scale linearly with the electric size of the block diameter [14], [17], which supports the proposed paper. In addition, a problem involving complicated materials is equivalent to the problem of equivalent currents radiating in the free space (or background material). Therefore, the same Green's function analyzed in this section applies, and hence the findings on the rank remain the same.

III. Numerical Validation of the Proposed Analytical Approach for Rank Study

We first quantitatively validate the proposed analytical approach for analyzing the rank of the IE operators by three representative examples. Through these examples, we also demonstrate the compressibility of the Fourier coefficients of Green's function numerically.

A. Example 1

The first example has a 1-D distribution of source and observer points. The source domain is in the range of $x' \in (-1.5A, -0.5A)$, while the observation domain is located at $x \in (0.5A, 1.5A)$. It is clear that $\vec{r} - \vec{r}' = (x - x', 0, 0)$ with $x - x' \in (A, 3A)$. The wavelength $\lambda = 1$ m, thus $k_0 = 2\pi$ in Green's function. The A is chosen as 4λ. A uniform discretization along x is used with a space step of Δ.

The Fourier transforms shown in (14) for sources, observations, and Green's function are performed in the range of (a_1, a_2) common to source region $\vec{r}'$, observer region $\vec{r}$, and $\vec{r} - \vec{r}'$ region, thus with $a_1 = -1.5A$ and $a_2 = 3A$. Hence, we

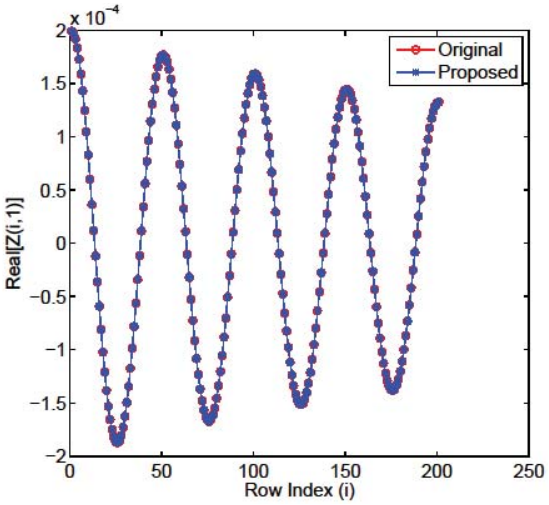

Fig. 2. Comparison between the matrix generated from the proposed approach and the original matrix for a line example in the real part of the first column of **Z**.

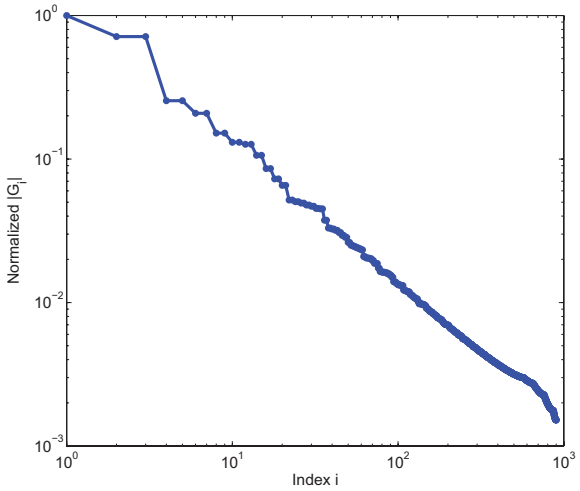

Fig. 3. Normalized magnitude of the entries of diagonal matrix **G** for the 1-D line distribution of sources and oberservers, which are the normalized Fourier coefficients of Green's function.

have the following:

$$B(k_i) = \int_{a_1}^{a_2} b(x) e^{-jk_i x}\, dx$$
$$F(k_i) = \int_{a_1}^{a_2} f(x') e^{-jk_i x'}\, dx'$$
$$G(k_i) = \int_{a_1}^{a_2} g(|x - x'|) e^{-jk_i (x-x')}\, d(x - x') \qquad (59)$$

with

$$k_i = i \frac{2\pi}{(a_2 - a_1)}, \quad i = 0, \pm 1, \pm 2, \ldots. \qquad (60)$$

The interval for integration (a_1, a_2) is chosen to carry out the discrete Fourier transforms of observations b, sources f, and Green's function g in a common range. The f, b, and g are padded with zeros in the range beyond where they are originally defined.

From (59), the diagonal matrix **G** is obtained with Fourier mode index $i \in [-ns/2+1, ns/2]$, where ns is the number of sampling points along x, which is $ns = (a_2 - a_1)/\Delta$. The **B** matrix and **F** matrix are constructed based on (18) and (20), where the line integral is performed with a simple center-point-based integration. Specifically, their ij-th element for this example is as follows:

$$\mathbf{B}_{i,j} = e^{-jk_i x_j} \Delta, \quad \mathbf{F}_{i,j} = e^{-jk_i x'_j} \Delta \qquad (61)$$

where x_j and x'_j are, respectively, the jth observation and source point, while i is the index of the Fourier mode. With **G**, **B**, **F** obtained, we construct $\mathbf{Z}^{t,s}$ based on (23), thus

$$\mathbf{Z}^{t,s} = (\mathbf{B}^{\mathrm{H}}\mathbf{B})^{-1}(\mathbf{B}^{\mathrm{H}}\mathbf{G}\mathbf{F}). \qquad (62)$$

To assess the accuracy of the proposed approach, we compare (62) with the original matrix that is directly constructed from the following:

$$\mathbf{Z}^{t,s}_{orig,ij} = \frac{e^{-jk_0|x_i - x'_j|}}{4\pi |x_i - x'_j|} \Delta. \qquad (63)$$

With a space step of $\Delta = 1/50\lambda$, the dimension of matrices **B** and **F** is both 900 by 200, and that of diagonal matrix **G** is 900 by 900. Thereby, $\mathbf{Z}^{t,s}$ is of size 200 by 200. In other words, there are 200 source points and 200 observation points, while the number of Fourier modes is 900. The number of Fourier modes is larger than the number of sources/observers because the region for performing Fourier transform is an extended region that contains all of the source region $\vec{r}'$, observer region $\vec{r}$, and $\vec{r} - \vec{r}'$ region. The size of this extended region, though larger, is linearly proportional to the maximum size of the source and the observer region. In addition, although **G**'s size is larger than the matrix size of $\mathbf{Z}^{t,s}$, we soon will show that **G** can be truncated to a size much smaller than that of $\mathbf{Z}^{t,s}$ based on prescribed accuracy, thus rendering $\mathbf{Z}^{t,s}$ low rank.

In Fig. 2, we plot the first column of the matrix obtained from (62) in comparison with that of the original matrix shown in (63). An excellent agreement can be observed. The same agreement is observed in all the other columns of the $\mathbf{Z}^{t,s}$ matrix. To assess the entire matrix error of (62), we evaluate the following matrix error:

$$\text{error} = \frac{\left\| \mathbf{Z}^{t,s}_{orig} - \mathbf{Z}^{t,s} \right\|}{\left\| \mathbf{Z}^{t,s}_{orig} \right\|} \qquad (64)$$

in which 2-norm is used. The error is shown to be 2.5769e-14. Hence, the accuracy of the factorized form shown in (62) is validated. Therefore, the rank of $Z^{t,s}$ is bounded from above by the rank of diagonal matrix **G**.

To demonstrate the compressibility of **G**, in Fig. 3, we plot the normalized magnitude of **G**'s entries sorted in a descending order, which are the normalized Fourier coefficients. It is evident that for a given accuracy, **G** can be truncated. As an example, we used 1% as a truncation criterion, and obtained a truncated **G** matrix. The rank of truncated **G** is shown to be 133, which is smaller than **G**'s original size 900, and also the size of $\mathbf{Z}^{t,s}$ that is 200. With the truncated **G**, we

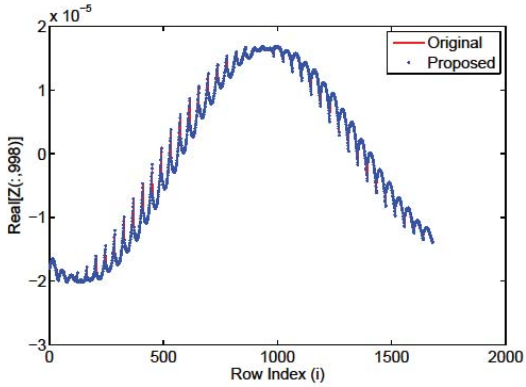

Fig. 4. Comparison between the matrix generated from the proposed approach and the original matrix for a plate example (Real part of the 998th column of $\mathbf{Z}$).

constructed the $\mathbf{Z}^{t,s}$ matrix based on (62). As $\mathbf{G}$ is low rank, $\mathbf{Z}^{t,s}$ is also low rank. The matrix error (64), which assesses the error of the low-rank approximation, is shown to be 0.46%. As another example, we used 5% as a truncation criterion to remove all entries of $\mathbf{G}$ whose normalized magnitude is <5%, the rank of $\mathbf{G}$ is found to be 25, which is much smaller than the size of $\mathbf{Z}^{t,s}$. Though a significant compression of the rank of $\mathbf{Z}^{t,s}$ from 200 to 25, good accuracy is still achieved since the resulting matrix error (64) is found to be only 2.74%.

We also repeat the aforementioned analysis by using a space step of $\Delta = 1/10\lambda$. In this case, the dimension of $\mathbf{B}$ and $\mathbf{F}$ becomes 180 by 40, and that of $\mathbf{G}$ is 180 by 180. The normalized $\mathbf{G}$'s elements are the same as those shown in Fig. 3, but with only 180 elements. With the complete $\mathbf{G}$, the entire matrix error of (64) is shown to be 5.54e-15. With a truncated $\mathbf{G}$ of only the 19 largest entries while setting the rest of $\mathbf{G}$'s elements to be zero, the error of (64) is shown to be 3.3%. It is evident that $\mathbf{G}$ can be truncated based on a desired accuracy, and the resulting $\mathbf{Z}^{t,s}$ is low rank.

B. Example 2

The second example is two separated plates that are horizontally displaced. One is located at $(0 \le x' \le A, 0 \le y' \le A, z' = 0)$, the other at $(3A \le x \le 4A, 0 \le y \le A, z = 0)$. It is clear that $\vec{r} - \vec{r}' = (x - x', y - y', 0)$ with $(x - x') \in (2A, 4A)$ and $(y - y') \in (-A, A)$. The wavelength is 1 m, thus $k_0 = 2\pi$ in Green's function. The A is chosen as 1 wavelength. A uniform discretization along both x and y is used with a space step Δ.

The Fourier transforms shown in (14) for sources, observations, and Green's function are performed in a common range of $(a_1, a_2) = (0, 4A)$, and $(b_1, b_2) = (-A, A)$. Thus, we have the following:

$$B(\vec{k}_i) = \int_{b_1}^{b_2}\int_{a_1}^{a_2} b(x,y)e^{-jk_{xi}x}e^{-jk_{yi}y}\,dx\,dy$$

$$F(\vec{k}_i) = \int_{b_1}^{b_2}\int_{a_1}^{a_2} f(x',y')e^{-jk_{xi}x'}e^{-jk_{yi}y'}\,dx'\,dy'$$

$$G(\vec{k}_i) = \int_{b_1}^{b_2}\int_{a_1}^{a_2} g(|x-x'|,|y-y'|)e^{-jk_{xi}(x-x')} \times e^{-jk_{yi}(y-y')}\,d(x-x')\,d(y-y') \quad (65)$$

where

$$k_{xi} = m\frac{2\pi}{(a_2-a_1)}, \quad k_{yi} = n\frac{2\pi}{(b_2-b_1)}, \quad m,n = 0,\pm1,\pm2,\ldots. \quad (66)$$

Based on (65), the diagonal matrix $\mathbf{G}$ is obtained with Fourier mode index $m \in (-nx/2+1, nx/2)$, and $n \in (-ny/2+1, ny/2)$, where nx is the number of sampling points along x which is $nx = (a_2 - a_1)/\Delta$, and ny is the number of sampling points along y which is $ny = (b_2 - b_1)/\Delta$. The $\mathbf{B}$ matrix and $\mathbf{F}$ matrix are constructed based on (18) and (20). Again, a straightforward center-point-based integration is used to calculate the surface integrals. Specifically, the ij-th element of $\mathbf{B}$ and $\mathbf{F}$ for this example is as follows:

$$\mathbf{B}_{i,j} = e^{-jk_{xi}x_j - jk_{yi}y_j}\Delta^2, \quad \mathbf{F}_{i,j} = e^{-jk_{xi}x'_j - jk_{yi}y'_j}\Delta^2. \quad (67)$$

We then construct $\mathbf{Z}^{t,s}$ based on (23), thus

$$\mathbf{Z}^{t,s} = (\mathbf{B}^{\mathrm{H}}\mathbf{B})^{-1}(\mathbf{B}^{\mathrm{H}}\mathbf{G}\mathbf{F}).$$

To assess the accuracy of the proposed approach, we compare the above with the original matrix that is directly constructed as the following:

$$\mathbf{Z}^{t,s}_{orig,ij} = \frac{e^{-jk_0\sqrt{(x_i-x'_j)^2+(y_i-y'_j)^2}}}{4\pi\sqrt{(x_i-x'_j)^2+(y_i-y'_j)^2}}\Delta^2. \quad (68)$$

With a space step of $\Delta = 1/40\lambda$, the dimension of $\mathbf{B}$ and $\mathbf{F}$ is both 12 800 by 1600, and that of $\mathbf{G}$ is 12 800 by 12 800, thus $\mathbf{Z}^{t,s}$ is of size 1600 by 1600. In Fig. 4, we plot a randomly selected column (column 998) of the matrix obtained from the proposed approach in comparison with that of the original matrix shown in (68), an excellent agreement can be observed. In addition, we compute (64) to assess the entire matrix error, which is shown to be 1.2429e-14. Again, the validity of the proposed method of using the Fourier analysis of Green's function to study the rank of an integral operator is demonstrated.

In Fig. 5, we plot the normalized magnitude of $\mathbf{G}$'s entries sorted in a descending order. It is clear that for a given accuracy, $\mathbf{G}$ can be truncated. We used 1% as a truncation criterion, and obtained a truncated $\mathbf{G}$ matrix, the size of which is shown to be 183 since the rest of the 12617 entries are all smaller than the maximum $\mathbf{G}$ value by 1%. With the truncated $\mathbf{G}$, we construct $\mathbf{Z}^{t,s}$ based on (62). The error of (64) is shown to be only 0.71%.

We also repeat the same study by using a space step of $\Delta = 1/10\lambda$. In this case, the dimension of $\mathbf{B}$ and $\mathbf{F}$ becomes 800 by 100, and that of $\mathbf{G}$ is 800 by 800. With the complete $\mathbf{G}$, the entire matrix error of (64) is shown to be 2.7522e-15. With a truncated $\mathbf{G}$ of only the 51 largest entries while setting the rest of $\mathbf{G}$'s elements to be zero based on a truncation criterion of 3%, the error of (64) is shown to be 2.63%. Once again, it demonstrates that $\mathbf{G}$ can be truncated based on a desired accuracy, and the resulting $\mathbf{Z}^{t,s}$ is low rank.

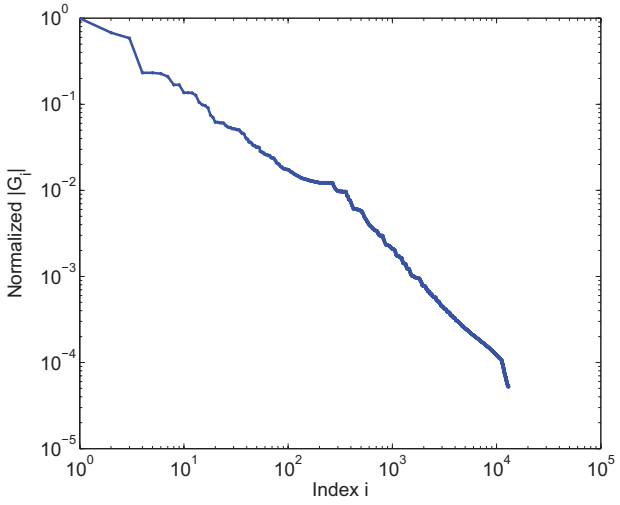

Fig. 5. Normalized magnitude of the entries of diagonal matrix **G** for two horizontally separated plates.

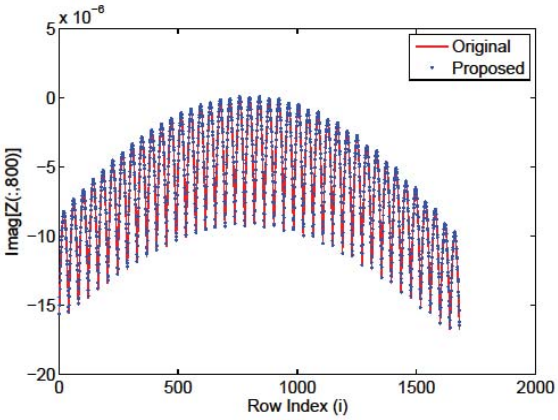

Fig. 6. Comparison between the matrix generated from the proposed approach and the original matrix for the second plate example (Imaginary part the 800th column of **Z**).

C. Example 3

We also consider the same two plates as simulated in the above example but displaced normally by $2A$. Thus, one plate is located at $(0 \le x' \le A, 0 \le y' \le A, z' = 0)$, while the other is at $(0 \le x \le A, 0 \le y \le A, z = 2A)$. This is a 3-D configuration of sources and observers. It is clear that $\vec{r} - \vec{r}' = (x - x', y - y', h)$ with $(x - x') \in (-A, A)$ and $(y - y') \in (-A, A)$. The other parameters are the same as used in the above example.

The Fourier transforms shown in (14) for sources, observations, and Green's function are performed in a common range of $(a_1, a_2) = (-A, A)$, and $(b_1, b_2) = (-A, A)$, and $(0, h = 2A)$. Different from (68), now the original matrix becomes

$$\mathbf{Z}^{t,s}_{orig,ij} = \frac{e^{-jk_0\sqrt{(x_i - x'_j)^2 + (y_i - y'_j)^2 + h^2}}}{4\pi\sqrt{(x_i - x'_j)^2 + (y_i - y'_j)^2 + h^2}}\Delta^2. \quad (69)$$

With a space step of $\Delta = 1/40\lambda$, the dimension of **B** and **F** is both 6400 by 1600, and that of **G** is 6400 by 6400. In Fig. 6, we plot the imaginary part of a randomly selected column (column 800) of the matrix obtained from the proposed approach in comparison with that of the original matrix shown in (69). An excellent agreement can be observed. In addition, we compute (64) to assess the entire matrix error, which is shown to be 8.0467e-15. In Fig. 7, we plot the normalized magnitude of **G**'s entries sorted in a descending order, which again reveals the compressibility of **G**. We used 1% as a truncation criterion, and obtained a truncated **G** matrix of size 33. With the truncated **G**, we recover the matrix based on (62). The error of (64) is shown to be 1%. We also repeat the same study by using a space step of $\Delta = 1/10\lambda$. In this case, the dimension of **B** and **F** becomes 400 by 100, and that of **G** is 400 by 400. With the complete **G**, the entire matrix error of (64) is 1.4756-15. With a truncated **G** based on 1% criterion, only the 45 largest entries need to be kept, yielding the error of (64) 0.78%.

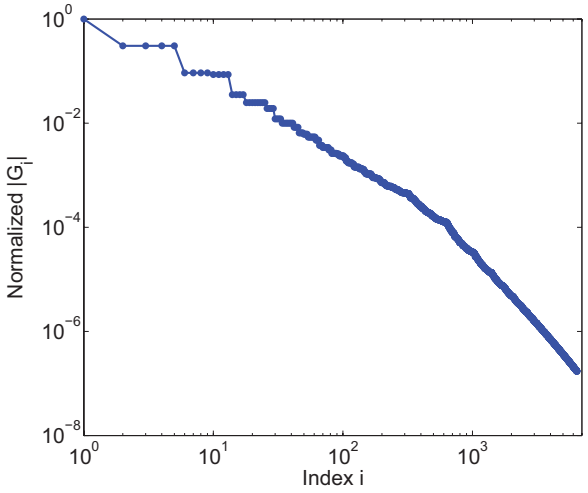

Fig. 7. Normalized magnitude of the entries of diagonal matrix **G** for two vertically separated plates.

In fact, performing a Fourier transform on a convolution integral is the technique underlying existing FFT-based IE solvers. Therefore, in addition to a theoretical proof developed in Section II-C, we also numerically prove that one can use **G**'s rank to analytically analyze the rank of an IE operator irrespective of the operator kind, object shape, and electric size.

IV. Numerical Validation of the Rank's Dependence With Electric Size

In Section II-D, we theoretically deduce the rank's growth rate with electric size from the Fourier transform of Green's function. In this section, we numerically validate our theoretical findings of the rank by performing an SVD to find out the minimal rank required by a given accuracy.

A. Two Separated Lines

The first example simulated has a 1-D distribution of sources and observers. It is the same as the example described in Section III-A, but the side length A is increased from 1λ to 100λ to study the rank's dependence with electric size. The dense matrix that characterizes the interaction between

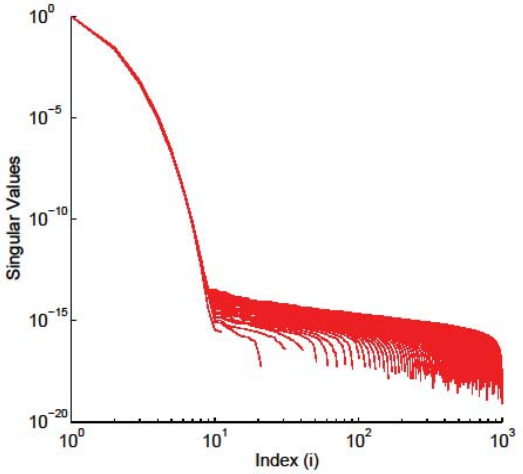

(a)

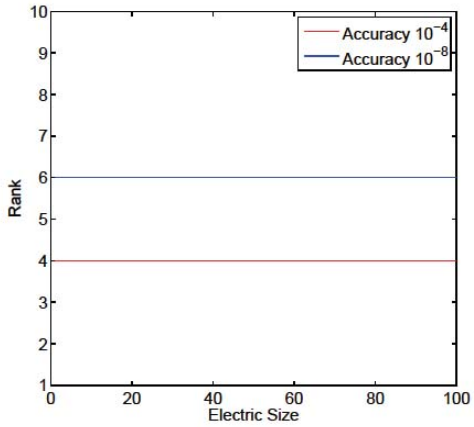

(b)

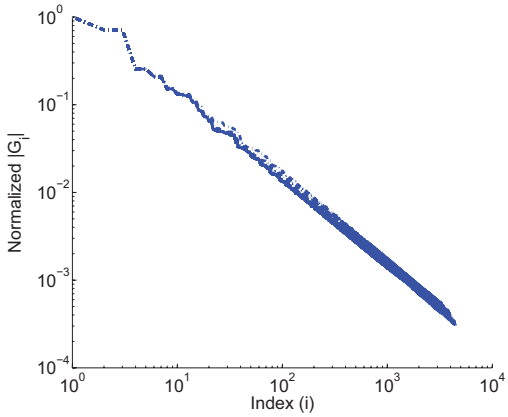

(c)

Fig. 8. Rank study of the interaction between two separated lines. (a) Singular value distributions for 100 different electric sizes from 1 to 100 wavelengths. (b) Rank for two accuracy requirements versus electric size. (c) Normalized Fourier coefficients of Green's function for 100 different electric sizes from 1 to 100 wavelengths.

the source line and the observation line has the following elements:

$$\mathbf{Z}_{ij} = \frac{e^{-jk_0|x_i - x'_j|}}{|x_i - x'_j|}. \tag{70}$$

The mesh density chosen is ten segments per wavelength. After constructing $\mathbf{Z}$ based on (70), we perform an SVD on $\mathbf{Z}$.

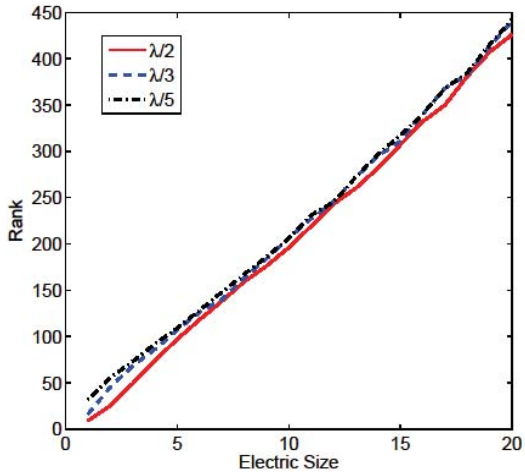

Fig. 9. Rank versus electric size generated with three different mesh densities.

In Fig. 8(a), we plot the normalized singular values sorted in a descending order obtained from 1λ to 100λ versus singular value index. There are 100 lines in this figure. However, they all overlap with each other above 10^{-14} accuracy. The singular values below 10^{-14} are more than 14 orders of magnitude smaller than the largest singular value. Because of machine precision, these singular values cannot be accurately obtained by computers, thus they differ from one simulation to the other simulation, and hence cannot be used to study the rank's growth with electric size. In Fig. 8(c), we plot the normalized Fourier coefficients of Green's function from 1 to 100 wavelengths. There are also 100 lines in this figure, which all overlap with each other. It is clear that the dependence of the rank with electric size determined from SVD agrees well with that found from the Fourier transform of Green's function.

In Fig. 8(b), we plot the rank of $\mathbf{Z}$ versus electric size for two different accuracy settings. The rank is determined by the number of singular values that satisfy the following criterion:

$$\frac{\sigma_i}{\sigma_1} \geq \varepsilon \tag{71}$$

where σ_i is the ith singular value, σ_1 is the largest singular value, and ε is the accuracy requirement, which is chosen as 10^{-4}, and 10^{-8}, respectively. It is clear that the rank is a constant regardless of electric size. This is not a surprising result since it is already shown by Fig. 8(a). As the singular-value lines for different electric sizes are all on top of each other, for a given accuracy, the resulting horizontal index, thus rank is the same for all electric sizes. Thus, the theoretical result shown in (56) is verified.

B. Two Configurations of a Plate-Plate Interaction

In the second example, we consider two separated plates in two configurations. In one configuration, the two plates are located in the same plane; whereas in the other configuration; one plate is normally displaced from the other plate. The two examples are the same as the two example described in Section III-B and -C, respectively. The only difference is that instead of having a fixed A, we increase A from 1λ to 60λ to study the rank's dependence with electric size.

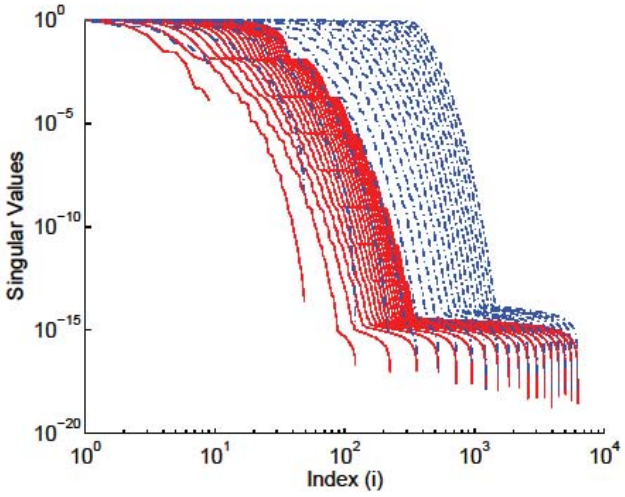

(a)

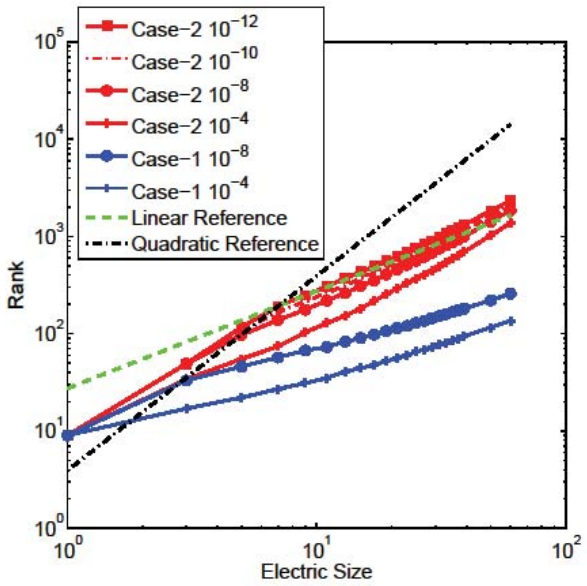

(b)

Fig. 10. Rank study of the interaction between two separated plates in two configurations. (a) Singular value distributions for 20 different electric sizes from 1 to 40 wavelengths with a step of two wavelengths (Red solid: Case 1 and Blue dashed: Case 2). (b) Rank versus electric size for both configurations required by different accuracy criteria.

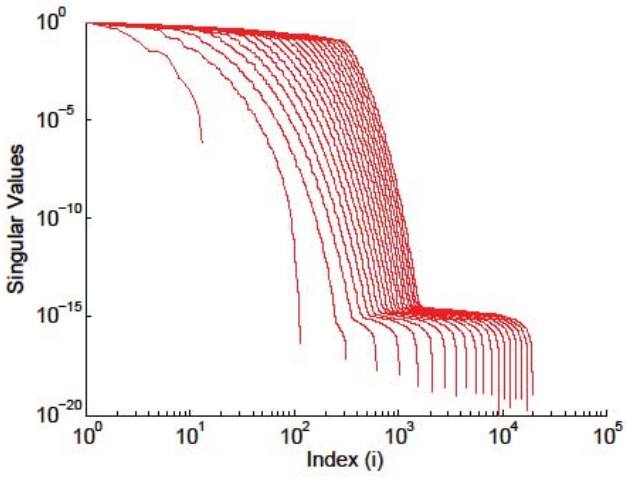

(a)

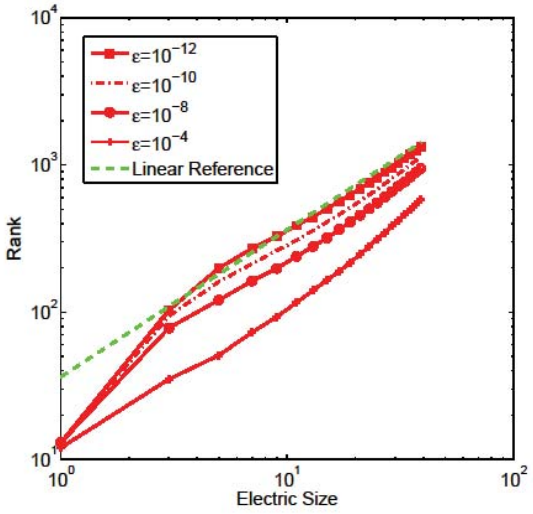

(b)

Fig. 11. Rank study of the interaction between two separated spheres. (a) Singular value distributions for 20 different electric sizes from 1 to 40 wavelengths with a spacing of two wavelengths. (b) Rank for four accuracy requirements versus electric size.

We first study the effect of mesh density on the rank's growth with electric size. As SVD is computationally intensive, it does not permit a fine discretization for studying a large electric size. If the effect of mesh density on the rank's growth rate is little, we can use a coarser mesh and, thereby a smaller matrix to study the rank for the same electric size. In Fig. 9, we plot the rank determined with $\varepsilon = 10^{-4}$ for this example versus electric size for three different mesh densities: $\lambda/2$, $\lambda/3$, and $\lambda/5$, respectively. As can be seen from this figure, the three lines are almost on top of each other. Therefore, in this and the example shown in next subsection, we use $\lambda/2$ as the mesh criterion so that larger electric sizes can be studied with SVD.

In Fig. 10(a), we plot the normalized singular values obtained from 1λ to 40λ versus singular value index. There are two sets of lines in this figure. The solid red lines correspond to the in-plane configuration of the two plates, whereas the dashed blue lines are the singular values of the normally displaced plate configuration. Each set has 20 lines representing singular values from 1λ, 3λ, $5\lambda, \ldots$, to 39λ, respectively, from left to right. It can be seen clearly that different from the 1-D case shown in the first example, when electric size increases, the entire singular value distribution is expanded to the right in both plate configurations, thus requiring more singular values and hence a larger rank to reach the same accuracy. However, for any given accuracy within machine precision, the rank for both configurations is shown to be less than the matrix size, which is the largest singular value index, as can be seen from Fig. 10(a). Therefore, the matrix has a low-rank property.

In Fig. 10(b), we plot the rank versus electric size of A from 1λ to 60λ for both configurations of the plates.

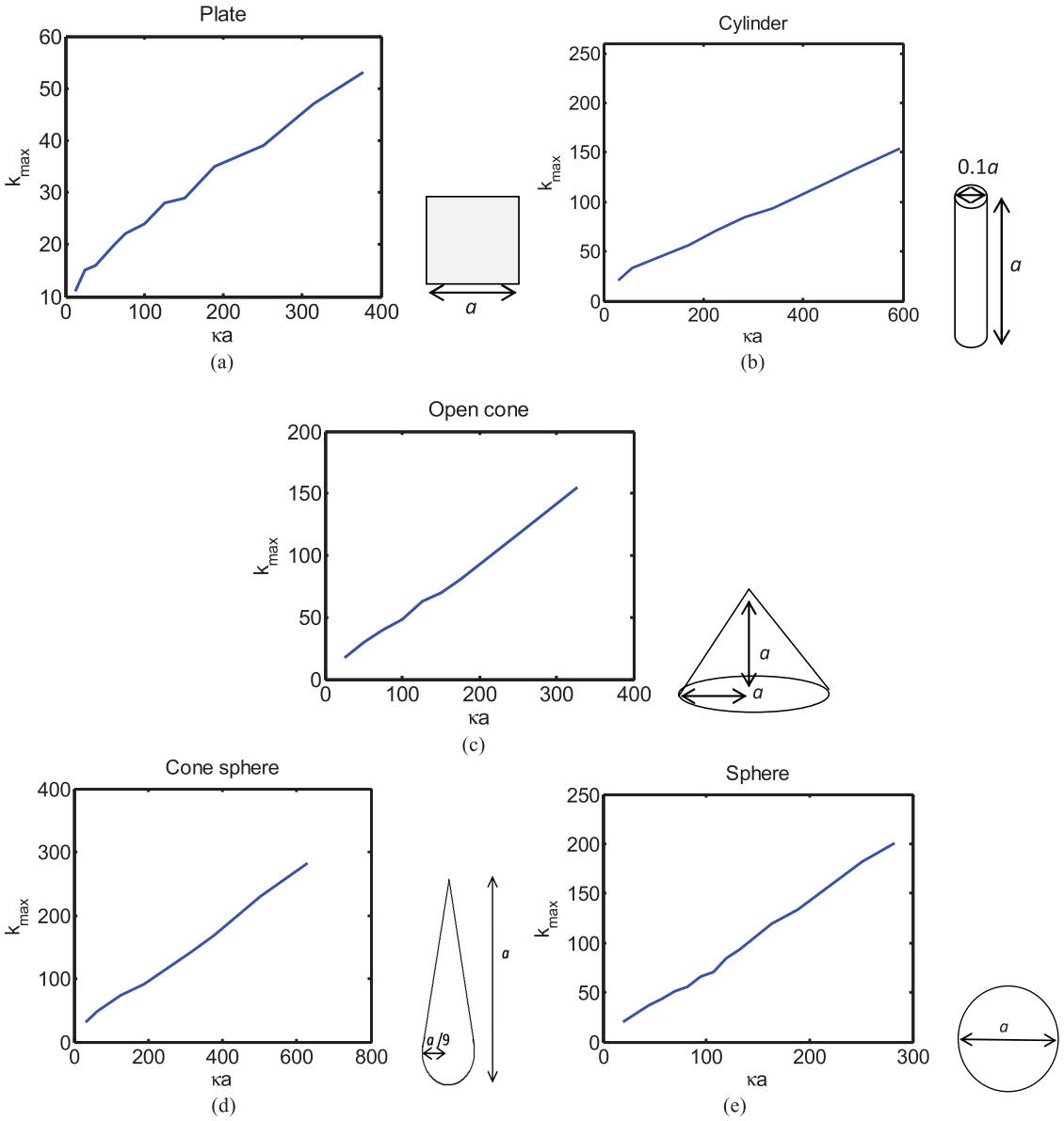

Fig. 12. Rank generated by ACA+ and SVD with respect to electric size for a variety of object shapes. (a) Plate. (b) Cylinder. (c) Open cone. (d) Cone sphere. (e) Sphere.

Case 1 represents the case where the two plates are on the same plane, while Case 2 is the other configuration. For Case 2, we plot the rank versus electric size for four different accuracy settings from $\varepsilon = 10^{-12}$, 10^{-10}, 10^{-8}, to 10^{-4}. The scaling of the rank is much closer to the linear scaling than to the quadratic scaling, both of which are shown in Fig. 10(b) for reference. It can also be seen that the scaling rate for a lower-order accuracy setting is larger than that of a higher-order accuracy setting. As for Case 1, the rank is shown to grow slowly with electric size. The growth rate is less than linear. It is clear that the rank required by Case 2 is larger than that in Case 1 for the same accuracy. This can be easily understood by comparing (69) with (68). The representation of Green's function in (69) requires more Fourier modes than that in (68) because h is involved, and its electric size increases. In Case 1, the Green's function for the two-plate interaction is solely determined by the 2-D x–y plane information, whereas in Case 2, the Green's function is contributed by the third dimension. Therefore, the growth rate of the rank with electric size for Case 1 is still governed by a 2-D-based growth rate that is less than linear, while the rank of Case 2 is closer to a 3-D-based rank.

C. Discussion

From Fig. 10(a), for case 2, it can be seen that there is fairly wide a range of index i within which the normalized singular values are quite flat. After this range, the normalized singular values drop rapidly. This phenomenon has been predicted by (35). The wavenumbers closest to k_0^2 have the largest singular values, and these wavenumbers distribute themselves on a spherical shell. If one stops at this range to observe the rank, he will get a quadratic growth with the electric size. However, the resultant error is very large. In other words,

by only keeping Fourier modes distributed on a spherical shell closest to k_0^2, the resultant error is too large to use. Therefore, one has to incorporate also those modes that have a certain distance away from k_0^2, i.e., inside a volume of a spherical ring with inner radius of k_0 and outer radius of $k_0+\Delta_k$ as shown by (52), to obtain an accurate representation of the integral operator. The height of this volume, Δ_k, is inversely proportional to frequency asymptotically. That is why the resultant rank is linearly proportional to frequency. In addition, one may observe the growth rate with electric size changes if different accuracy requirements are set, as shown by Fig. 10(b). It is also higher than linear when the accuracy setting is low. That is because the growth rate has not converged yet. One can increase the accuracy setting until the growth rate does not increase any more. Upon convergence, the growth rate is linear, which is proved by the theoretical bound of Δ_k.

D. Two Separated Spheres

In the third example, we consider two separated spheres. One sphere is centered at the origin with diameter A, and the other is centered at $(2A, 0, 0)$ with the same diameter. The λ is 1 m, and A is increased from 1λ to 40λ. The mesh density is $\lambda/2$. The sources and observers are located on the spherical surface. The matrix corresponding to the source-observation interaction has the following element:

$$\mathbf{Z}_{ij} = \frac{e^{-jk_0|\vec{r}_i-\vec{r}'_j|}}{|\vec{r}_i-\vec{r}'_j|}. \tag{72}$$

The matrix size, which is the number of sources (column dimension of the matrix) as well as the number of observers (row dimension of the matrix), ranges from 13, 315, 1018, 2124, to 17 204 when the electric size of the sphere diameter A increases from 1λ to 40λ. The SVD is then used to compute the rank of matrix $\mathbf{Z}$ for a given accuracy. In Fig. 11(a), we plot the normalized singular values obtained from 1λ to 40λ with a spacing of 2λ versus singular value index. There are 20 lines in this figure. The singular value lines are shown to expand to the right when electric size increases. In Fig. 11(b), we plot the rank of $\mathbf{Z}$ versus electric size for four different accuracy settings. The linear scaling line is also plotted for reference. As can be seen, the growth rate of the rank with electric size agrees very well with linear scaling.

E. Suite of Electrically Large Examples

To further verify the proposed theoretical analysis, we numerically determined the rank of a plate, cylinder, open cone, cone sphere, and sphere, resulting from a surface-based electric field integral operator by ACA+ [1], [8] and SVD from small to very large electric sizes. A detailed description of this scheme can be found from [5] and Section IV-A in [6]. Basically, we first use ACA+ to obtain a factorized low-rank form, and then perform an SVD on the factorized form to find out the minimal rank required by accuracy. The ACA+ is used because a direct SVD is very expensive when matrix size is large. For all these examples at all the electric sizes we simulate, a mesh size of 0.1λ is used. The RWG bases are used to expand unknown current and Galerkin scheme is used for testing. By an $\mathcal{H}$-matrix partition scheme (Section II-D in [6]), we partition the dense system matrix into admissible blocks and inadmissible blocks level by level. The admissible blocks are blocks that satisfy $\max\{\mathrm{diam}(\Omega_t), \mathrm{diam}(\Omega_s)\} \leq \eta\,\mathrm{dist}(\Omega_t, \Omega_s)$, where $\eta = 1$ is used. In an $\mathcal{H}$ matrix, the admissible blocks are represented by low-rank matrices, while inadmissible blocks are stored in a full matrix format. The leafsize used for the multilevel tree construction in the $\mathcal{H}$-matrix partition is 32. The error used in ACA+ and SVD truncation is 10^{-4}. We then find the maximal rank $k_{\max}$ among all the admissible blocks at all tree levels for each example simulated. It is clear that $k_{\max}$ corresponds to the rank of the matrix block that has the largest electric size in each example. In Fig. 12, we plot the $k_{\max}$ versus electric size for all of the five different objects. As can be seen clearly, $k_{\max}$ is O(ka). Thus, it verified the proposed theoretical analysis.

V. Conclusion

A theoretical study was conducted in this paper to analyze the minimal rank of integral operators encountered in electromagnetic analysis and its dependence with electric size for a prescribed error bound. We highlighted the fact that the rank generated by SVD is the minimal rank required by accuracy. The SVD-based low-rank approximation does not rely on the separation of observation and source coordinates for separated geometry blocks, while methods that separate observers and sources such as interpolation and plane wave expansion-based methods do not lead to a minimal rank approximation of the electrodynamic kernel. Therefore, the rank obtained from these methods is observed to scale with electric size at a much higher rate.

The SVD analysis is numerical, which prevents a study of the rank for an arbitrarily large electric size. By recognizing the relationship between an SVD analysis and a Fourier analysis in a linear and shift-invariant system, we successfully developed an analytical approach to analyze the rank of an integral operator, and revealed the relationship between the rank and the electric size for satisfying a prescribed accuracy. The rank of the interaction between two separated geometry blocks was shown to scale linearly with the electric size of the block diameter in a general 3-D problem. As long as the rank is smaller than the matrix dimension, the matrix is low-rank. We thus theoretically proved the existence of an error bounded low-rank representation of electrodynamic integral operators irrespective of electric size and object shape. In addition, numerous results were generated to validate both the proposed analytical approach for analyzing the rank and the findings of this paper on the rank's asymptotic dependence with electric size.

The proof developed in this paper provided a theoretical basis for employing and further developing low-rank matrix algebra for accelerating the integral-equation-based computation of integrated circuits and systems from small to very large

electric sizes. It is also applicable to the analysis of other engineering problems, the physical phenomena of which are governed by Maxwell's equations.

REFERENCES

[1] S. Börm, L. Grasedyck, and W. Hackbusch, "Hierarchical matrices," (Lecture Notes on Mathematics in the Sciences). Leipzig, Germany: Inselstrasse, 2003.

[2] S. Börm, "$\mathcal{H}^2$-matrices—multilevel methods for the approximation of integral operators," *Comput. Vis. Sci.*, vol. 7, nos. 3–4, pp. 173–181, 2004.

[3] W. Hackbusch, B. Khoromskij, and S. Sauter, "On $\mathcal{H}^2$-matrices," (Lecture Notes on Applied Mathematics). Berlin, Germany: Springer-Verlag, 2000, pp. 9–29.

[4] W. Chai and D. Jiao, "An $\mathcal{H}^2$-matrix-based integral-equation solver of reduced complexity and controlled accuracy for solving electrodynamic problems," *IEEE Trans. Antennas Propag.*, vol. 57, no. 10, pp. 3147–3159, Oct. 2009.

[5] W. Chai and D. Jiao, "A complexity-reduced H-matrix based direct integral equation solver with prescribed accuracy for large-scale electrodynamic analysis," in *Proc. IEEE Int. Symp. Antennas Propag.*, Jul. 2010, pp. 1–4.

[6] W. Chai and D. Jiao, "A complexity-reduced H-matrix based direct integral equation solver with prescribed accuracy for large-scale electrodynamic analysis," School Electr. & Comput. Eng., Purdue Univ., Purdue, IN, USA, Tech. Rep. TR-ECE-11-04, Jul. 2010.

[7] W. Chai and D. Jiao, "Dense matrix inversion of linear complexity for integral-equation based large-scale 3-D capacitance extraction," *IEEE Trans. Microw. Theory Techol.*, vol. 59, no. 10, pp. 2404–2421, Oct. 2011.

[8] M. Bebendorf, "Approximation of boundary element matrices," *Numer. Math.*, vol. 86, no. 4, pp. 565–589, 2000.

[9] C. F. Van Loan and G. H. Golub, *Matrix Computations*. Baltimore, MD, USA: Johns Hopkins, 1996.

[10] H. H. Barrett and K. J. Myers, *Foundations of Image Science*. New York, NY, USA: Wiley, 2004.

[11] S. Park, J. M. Witten, and K. J. Myers, "Singular vectors of a linear imaging system as efficient channels for the Bayesian ideal observer," *IEEE Trans. Med. Imag.*, vol. 28, no. 5, pp. 657–668, May 2009.

[12] H. Liu and D. Jiao, "A theoretical study on the rank's dependence with electric size of the inverse finite element matrix for large-scale electrodynamic analysis," in *Proc. IEEE Int. Symp. Antennas Propag.*, Jul. 2012, pp. 1–2.

[13] C.-T. Tai, *Dyadic Green Functions in Electromagnetic Theory*, 2nd ed. Piscataway, NJ, USA: IEEE Press, 1993.

[14] W. C. Chew, J. M. Jin, E. Michielssen, and J. M. Song, *Fast and Efficient Algorithms in Computational Electromagnetics*. Norwood, MA, USA: Artech House, 2001.

[15] W. Chai and D. Jiao, "An LU decomposition based direct integral equation solver of linear complexity and higher-order accuracy for large-scale interconnect extraction," *IEEE Trans. Adv. Packag.*, vol. 33, no. 4, pp. 794–803, Nov. 2010.

[16] A. F. Peterson, "The interior resonance problem associated with surface integral equations of electromagnetics: Numerical consequences and a survey of remedies," *Electromagn.*, vol. 10, no. 3, pp. 293–312, Jul.–Sep. 1990.

[17] V. Rokhlin, "Diagonal forms of translation operators for the Helmholtz equation in three dimensions," *Appl. Comput. Harmon. Anal.*, vol. 1, pp. 82–93, Dec. 1993.

[18] L. Tsang, J. A. Kong, and K. Ding, *Scattering of Electromagnetic Waves, Theories and Application*. New York, NY, USA: Wiley, 2000.

[19] W. Chai and D. Jiao, "Direct matrix solution of linear complexity for surface integral-equation based impedance extraction of complicated 3-D structures," *Special Issue on Large Scale Electromagnetic Computation for Modeling and Applications, Proc. IEEE*, vol. 101, no. 2, pp. 372–388, Feb. 2013.

[20] O. M. Bucci, C. Gennarelli, and C. Savarese, "Representation of electromagnetic fields over arbitrary surfaces by a finite and nonredundant number of samples," *IEEE Trans. Antennas Propag.*, vol. 46, no. 3, pp. 351–359, Mar. 1998.

Wenwen Chai (S'09) received the B.S. degree from the University of Science and Technology of China, Hefei, China, in 2004, the M.S. degree from the Chinese Academy of Sciences, Beijing, China, in 2007, and the Ph.D. degree from Purdue University, West Lafayette, IN, USA, in 2012, all in electrical engineering.

She was a Research Assistant with the On-Chip Electromagnetics Group, Purdue University, from 2007 to 2012. In 2012, she joined Synopsys Inc., Santiago, Chile, as a Senior R&D Engineer with the PrimeRail Group. Her current research interests include computational electromagnetics, high-performance VLSI CAD, and fast and high-capacity numerical methods.

Dr. Chai received the IEEE Antennas and Propagation Society Doctoral Research Award from 2009 to 2010 and Synopsys IG division Individual Recognition Award in 2012 for the contribution to the performance improvement of the large-scale power grid analysis tool.

Dan Jiao (S'00–M'02–SM'06) received the Ph.D. degree in electrical engineering from the University of Illinois at Urbana-Champaign, Urbana, IL, USA, in 2001.

She was with the Technology Computer-Aided Design (CAD) Division, Intel Corporation, Santa Clara, CA, USA, in September 2005, as a Senior CAD Engineer, a Staff Engineer, and a Senior Staff Engineer. In September 2005, she joined Purdue University, West Lafayette, IN, USA, as an Assistant Professor with the School of Electrical and Computer Engineering, where she is currently a Professor. She has authored two book chapters and over 170 papers in refereed journals and international conferences. Her current research interests include computational electromagnetics, high-frequency digital, analog, mixed-signal, and RF integrated circuit design and analysis, high-performance VLSI CAD, modeling of microscale and nanoscale circuits, applied electromagnetics, fast and high-capacity numerical methods, fast time-domain analysis, scattering and antenna analysis, RF, microwave, and millimeter-wave circuits, wireless communication, and bio-electromagnetics.

Dr. Jiao has served as the reviewer for many IEEE journals and conferences. She is an Associate Editor of the IEEE TRANSACTIONS ON COMPONENTS, PACKAGING, AND MANUFACTURING TECHNOLOGY. She received the 2013 S. A. Schelkunoff Prize Paper Award of the IEEE Antennas and Propagation Society, which recognizes the Best Paper published in the IEEE TRANSACTIONS ON ANTENNAS AND PROPAGATION. She was among the 85 engineers selected throughout the nation for the National Academy of Engineering's 2011 U.S. Frontiers of Engineering Symposium. She was a recipient of the 2010 Ruth and Joel Spira Outstanding Teaching Award, the 2008 National Science Foundation CAREER Award, the 2006 Jack and Cathie Kozik Faculty Start up Award (which recognizes an Outstanding New Faculty Member of the School of Electrical and Computer Engineering, Purdue University), the 2006 Office of Naval Research Award under the Young Investigator Program, the 2004 Best Paper Award presented at the Intel Corporation's Annual Corporate-Wide Technology Conference (Design and Test Technology Conference) for her work on generic broadband model of high-speed circuits, the 2003 Intel Corporation's Logic Technology Development (LTD) Divisional Achievement Award in recognition of her work on the industry-leading BroadSpice modeling/simulation capability for designing high-speed microprocessors, packages, and circuit boards, the Intel Corporation's Technology CAD Divisional Achievement Award for the development of innovative full-wave solvers for high frequency IC design, the 2002 Intel Corporation's Components Research the Intel Hero Award (Intel-wide she was a tenth recipient) for the timely and accurate 2-D and 3-D full-wave simulations, the Intel Corporation's LTD Team Quality Award for her outstanding contribution to the development of the measurement capability and simulation tools for high frequency on-chip crosstalk, and the 2000 Raj Mittra Outstanding Research Award by the University of Illinois at Urbana-Champaign.